TITANIUM NITRIDE PRECIPITATION BEHAVIOR IN THIN-SLAB CAST HSLA STEELS

by

Michael T. Nagata

A thesis submitted to the Faculty and the Board of Trustees of the Colorado School of Mines in partial fulfillment of the requirements for the degree of Master of Science (Metallurgical and Materials Engineering).

Golden, Colorado

Date 18th June, 2001

Signed: _____

Michael T. Nagata

Approved: _____

Dr. John G. Speer

Golden, Colorado

Date 6/18/01

_____

Dr. John J. Moore
Department Chairman
Department of Metallurgical and
Materials Engineering

ABSTRACT

To assess the potential for obtaining and utilizing titanium nitride (TiN) refinement via the increased post-solidification cooling rates associated with thin-slab casting (TSC), TiN particle size distributions were evaluated by TEM examination of carbon extraction replicas. Seven commercially produced thin-slab cast TiN steels, one thin-slab cast Ti-free steel, and one conventionally cast steel were received. Thin slab samples were taken from three locations in the production process: quenched after casting before the tunnel furnace, quenched after tunnel furnace soaking, and the as-rolled and air cooled final product.

Effects of cooling rate were evident in the results and agree with previously documented behavior, where precipitate size decreases with increased cooling rate. Statistical differences in particle size between specimens from steels with different chemistries were shown. These variations result from differences in the driving force for precipitation, rates of coarsening, and differences in volume fraction due to changes in steel composition. The interaction of composition and processing, such as soaking in the tunnel furnace and rolling, was found to be important. For example, the hyperstoichiometric steel (excess Ti), exhibited fine TiN after casting and soaking, but dramatic coarsening after hot-rolling. This behavior was attributed to deformation enhanced particle coarsening, and/or incomplete precipitation after soaking, followed by continued growth during subsequent processing.

Specimens were heat treated over a range of temperatures in order to study the prior austenite grain coarsening process and the influence of varying the TiN distribution. Three stages of grain growth were observed, similar to other TiN technology steels. Large differences in grain coarsening temperature between the different Ti-added steels was not observed, despite the different TiN dispersions.

Ferrite grain size was measured in the final hot-rolled product to assess whether TiN influenced the thermomechanical processing response. Both TiN containing and Ti-free steels were examined, and despite considerable variations in TiN size along with evidence of further precipitation during the rolling process for some steels, it was apparent that the austenite pinning effects were overshadowed by the refinement resulting from hot-rolling of the thin slabs.

TABLE OF CONTENTS

ABSTRACT iii
TABLE OF CONTENTS iv
LIST OF FIGURES vi
LIST OF TABLES x
ACKNOWLEDGEMENTS xi
1.0 BACKGROUND 1
1.1 Introduction 1
1.2 Thin-Slab Casting 2
1.2.1 Physical Description 2
1.2.2 Casting of Liquid Steel 3
1.2.3 Solid-State Processing 5
1.3 Titanium Nitride Technology 7
1.4 Grain Coarsening 13
1.5 Use of Extraction Replicas for Precipitation Studies 17
2.0 EXPERIMENTAL METHODS 20
2.1 Alloy Design and Material Acquisition 20
2.2 Precipitate Study 24
2.3 Prior Austenite Grain Coarsening Study 25
2.4 Ferrite Grain Size Study 26
2.5 Statistical Analysis 27
2.5.1 Analysis of Variance (ANOVA) 27
2.5.2 Multiple Comparison Procedures (MCP) 29
2.5.3 Application of Statistical Techniques 31
3.0 RESULTS AND DISCUSSION 32
3.1 Precipitate Size Study 32
3.1.1 Chemistry Effects 34

3.1.1.1 As-Cast Condition 35
3.1.1.2 After-Furnace Condition 36
3.1.1.3 End Product Condition 39
3.1.2 Effects of Sampling Location 41
3.1.2.1 After-Caster 42
3.1.2.2 After-Furnace 43
3.1.3 Processing Effects 45
3.1.3.1 Effects of Tunnel Furnace 45
3.1.3.2 Effects of Rolling Process 48
3.1.4 Casting Method - Conventional vs. Thin Slab 55
3.2 Austenite Grain Coarsening Study 58
3.3 Ferrite Grain Size in End Product 63
3.4 Implications 65
4.0 CONCLUSIONS 67
5.0 REFERENCES 69
6.0 APPENDIX A 73
7.0 APPENDIX B 76
8.0 APPENDIX C 81
9.0 APPENDIX D 85

LIST OF FIGURES

Figure 1.1 Funnel-shaped mold with submerged casting nozzle.. 3

Figure 1.2 Schematic representation of thin-slab casting process.. 3

Figure 1.3 Effect of deformation on degree of recrystallization of coarse austenite for interpass times of one or two seconds. 6

Figure 1.4 Austenite evolution during hot rolling of 50mm thick slab to a final thickness of 6 mm.. 7

Figure 1.5 Increasing microalloy additions increase grain coarsening temperature. 8

Figure 1.6 Relationship between grain size, R, particle size, r, and volume fraction, f_v, as predicted by three models. 9

Figure 1.7 Effect of post-solidification cooling rate on TiN particle size. 10

Figure 1.8 Solubility diagram showing how moving to a hypostoichiometric Ti:N ratio will decrease the amount of titanium left in solution. 11

Figure 1.9 Solvus temperature of precipitates increase as composition moves away from stoichiometric line. 13

Figure 1.10 Effect of various microalloying elements on austenite grain growth and grain coarsening temperature. 14

Figure 1.11 Schematic diagram of model for grain coarsening temperature (GCT).. 15

Figure 1.12 Solubilities of microalloy carbides and nitrides in austenite. 16

Figure 1.13 Effect of as-reheated grain size on the microstructure evolution of Ti-V austenite during an otherwise identical rolling schedule.. 17

Figure 1.14 Ferrite refinement with increased cooling rate.. 17

Figure 1.15 Cumulative distribution plot of particle sizes for three different alloys. 19

Figure 2.1 Solubility plot showing design matrix of steels 20

Figure 2.2 Solubility plot showing steels received for investigation. 22

Figure 2.3 Schematic of sampling locations in thin-slab casting process. 23

Figure 3.1 STEM photomicrograph of TiN particles in Steel [4] 0.022Ti, 0.016N in the end product condition. 33

Figure 3.2 EDS results of TiN precipitate from Steel [4] 0.022Ti, 0.016N. 34

Figure 3.3 Mean TiN particle size and 95% confidence interval for as-cast samples. 35

Figure 3.4 Solubility plot with mean particle sizes for as-cast samples. 36

Figure 3.5 Mean TiN particle size and 95% confidence interval for after-furnace sample. 37

Figure 3.6 Solubility plot with mean particle sizes for after-furnace samples. 38

Figure 3.7 Mean TiN particle size and 95% confidence interval for end product samples. 39

Figure 3.8 Solubility plot with mean particle sizes for end product samples. 40

Figure 3.9 Mean TiN particle size and 95% confidence interval for surface and centerline of after-caster slab conditions. 42

Figure 3.10 Photomicrographs of TiN precipitates in Steel [2] from after-caster condition (STEM). A) Centerline and B) Surface. 43

Figure 3.11 Mean TiN particle size and 95% confidence interval for surface and centerline of after-furnace slab conditions. 44

Figure 3.12 Photomicrographs of TiN precipitates in steel [2] from after-furnace condition (STEM). A) Centerline and B) Surface. 44

Figure 3.13 Mean TiN particle size and 95% confidence interval at centerline of after-caster and after-furnace slab products. 46

Figure 3.14 Solubility plot comparing mean particle sizes for after-caster and after-furnace conditions. 46

Figure 3.15 Photomicrographs of TiN precipitates in steel [1] 0.009Ti, 0.014N (STEM). From centerline of: A) After-caster and B) After-furnace. 47

Figure 3.16 Photomicrographs of TiN precipitates in steel [2] 0.008Ti, 0.009N (STEM). From centerline of: A) After-caster and B) After-furnace. 47

Figure 3.17 Mean TiN particle size and 95% confidence interval of end product and after-furnace slab condition (centerline). 49

Figure 3.18 Solubility plot comparing mean particle sizes for end product and after-furnace samples. 50

Figure 3.19 Photomicrographs of TiN precipitates in steel [1] 0.009Ti, 0.014N (STEM). A) After-furnace (centerline) and B) End product. 50

Figure 3.20 Photomicrographs of TiN precipitates in steel [2] 0.008Ti, 0.009N (STEM). A) After-furnace (centerline) and B) End product. 51

Figure 3.21 Photomicrographs of TiN precipitates in steel [4] 0.022Ti, 0.016N (STEM). A) After-furnace and B) End product. 51

Figure 3.22 Photomicrographs of TiN precipitates in steel [5] 0.021Ti, 0.013N (STEM). A) After-furnace and B) End product. 52

Figure 3.23 Photomicrographs of TiN precipitates in steel [6] 0.011Ti, 0.009N (STEM). A) After-furnace and B) End product. 52

Figure 3.24 Particle size distributions showing cold charge rolling (CCR) and hot direct rolling (HDR). 53

Figure 3.25 Photomicrographs of TiN precipitates in the hyperstoichiometric steel [3] (STEM). A) After-furnace and B) End product. 54

Figure 3.26 Mean TiN particle size and 95% confidence interval at centerline of the after-caster slab product for thin slab and thick slab cast steels. 56

Figure 3.27 Photomicrographs of TiN precipitates in the conventional cast steel [10] (STEM). A) Centerline and B) Surface. 57

Figure 3.28 Change in particle size distribution during coarsening, represented by relative probability, hi, as a function of mean intercept length, L. Results are for Sn-rich Pb-Sn system. 57

Figure 3.29 Examples of prior austenite grain boundary photomicrographs. A) [10] Thick Slab and B) [2] 0.008Ti, 0.009N austenitized at 900oC. 58

Figure 3.30 Range of results of austenite grain coarsening study for thin slab cast TiN steels. . 59

Figure 3.31 Summary "envelope" of results of austenite grain study for the thin slab cast TiN steels. 60

Figure 3.32 Range of results of austenite grain coarsening study for thin slab cast TiN steels (shaded) and the result from thick slab cast TiN steel. 62

Figure 3.33 Range of results of austenite grain coarsening study for thin slab cast TiN steels and the result from the Ti-Free thin slab cast steel. 62

Figure 3.34 Example photomicrograph of ferrite grains in hot-rolled steel [2] 0.008Ti, 0.009N. 64

Figure 3.35 Ferrite grain size results. 64

Figure 3.36 Comparison of microstructure evolution in C-Mn and Ti-V austenite subjected to same rolling schedule. 65

Figure D.1 Prior-austenite grain study results for steel [1] 0.009Ti, 0.014N. 86

Figure D.2 Prior-austenite grain study results for steel [2] 0.008Ti, 0.009N. 87

Figure D.3 Prior-austenite grain study results for steel [3] 0.048Ti, 0.008N. 87

Figure D.4 Prior-austenite grain study results for steel [4] 0.022Ti, 0.016N. 88

Figure D.5 Prior-austenite grain study results for steel [7] 0.014Ti, 0.013N. 88

Figure D.6 Prior-austenite grain study results for steel [9] Ti-Free. 89

Figure D.7 Prior-austenite grain study results for steel [10] 0.015Ti, 0.006N. 89

LIST OF TABLES

Table 2.1 Matrix of Proposed Steels 20

Table 2.2 Chemical Composition (Product Analysis) of Thin-Slab Cast Steels 22

Table 2.3 Chemical Composition of Conventionally-Cast Steel [10] 23

Table 2.4 Thickness of As-Rolled Final Product Samples 23

Table A.1 Descriptive Statistics for TiN Precipitate Study 74

Table B.1 Tukey-Kramer Results for After-Caster Condition 77

Table B.2 Tukey-Kramer Results for After-Furnace Condition 78

Table B.3 Tukey-Kramer Results for End Product Condition 78

Table B.4 Results of t-tests for Surface/Centerline Differences 79

Table B.5 Results of t-tests for Comparison of After-Caster and After-Furnace Particle Size . . 79

Table B.6 Results of t-tests for Comparison of After-Furnace and End Product Particle Size . . 80

Table C.1 Descriptive Statistics for Prior-Austenite Grain Boundary Study 82

ACKNOWLEDGEMENTS

I would like to take this opportunity to thank a few of the many people that helped during my time at CSM, making the experience easier and more enjoyable.

Many thanks go to my thesis committee for their time and knowledge that were needed in the research and writing of this thesis. I would particularly like to thank my advisor, Dr. John Speer, for seeing me through this undertaking and helping me understand many aspects of my project.

I would like to thank the National Science Foundation and the sponsors of the Advanced Steel Processing and Products Research Center for funding this project. I appreciate the interactions with many sponsors from both the Plate and Sheet Steel Groups that offered additional ideas for my work. I would like to thank Rick Bodnar from Bethlehem Steel taking an active part as my industry sponsor contact, providing materials, guidance, and technical support in several areas of this project. I would like to thank Nucor Steel, especially Lynn Ondrovic, Nathan Fraser, and Donna Demark for providing me with the special materials for this project and answering all of my questions.

I would like to thank Dr. Gus Greivel of the Mathematical and Computer Sciences Department at CSM for his help with the statistical analysis needed in the project. I thank Bob McGrew for his continuous help in the electron microscope lab. Thanks to Tanya Quintana, who put in many hours to provide the etched specimens for the austenite grain coarsening study.

Finally, I would like to thank my friends, who kept my life interesting throughout my time at CSM. I would like to thank Q for lending me his statistical knowledge and Jim for lending me his office space.

1.0 BACKGROUND

1.1 Introduction

Thin-slab casting (TSC) is being used increasingly as a means of producing sheet steels due to its reduced capital costs. Although initial difficulties due to differences in production methods have been overcome, and a viable product is being produced, much remains unknown about this relatively new technology. Some metallurgical factors linked to thin-slab casting include faster post-solidification cooling rates, less time at very high temperatures, and direct charging after the caster, when compared to conventional casting. These intrinsic differences may provide an opportunity to control microstructure and properties in new ways through processing and chemistry.

One aspect in need of investigation is the formation of precipitates in the steel, with the aim of reducing particle size. There may be potential for obtaining and utilizing titanium nitride (TiN) refinement via the increased post-solidification cooling rates associated with thin-slab casting. The differences between conventional casting and thin-slab casting may conceivably change the effective solubility and coarsening behavior of TiN precipitates. Smaller precipitates are desirable because they are believed to be beneficial in retarding grain growth. The influences of steel composition on TiN size distribution in TSC material is of interest in that it may lead to the identification of a more "optimum" steel chemistry approach.

Changes in liquidus/solidus temperatures and cooling rate may influence the amount of TiN which may be precipitated in the solid, and the temperatures over which precipitation occurs, again influencing alloy design. As TiN precipitation behavior varies, the influence on austenite during thermomechanical processing will change and examination of austenite grain coarsening temperatures relating to TiN particle size is of interest.

This study was designed to improve the fundamental understanding of TiN technology in steels produced via thin slab casting. Titanium nitride particle size distributions and coarsening kinetics were to be examined in steels with varying Ti:N ratios to characterize the response to thin slab casting. Thin-slab cast steels were initially designed with different Ti:N ratios in order to

assess the effects of chemistry changes on TiN distributions. The details of the alloy design will be presented in a later section. Samples were taken at three locations during processing of the steel, to investigate the evolution of TiN precipitates. One conventionally cast Ti-containing steel was obtained in order to compare between the two production practices. The ferrite grain size (as-hot-rolled) and the austenite grain coarsening behavior of these steels were also examined, to relate the TiN precipitate variations to possible variations in final microstructure.

The following sections provide a review of some of the more important concepts related to this project, including thin-slab casting, TiN technology, and extraction replicas.

1.2 Thin-Slab Casting

1.2.1 Physical Description

Throughout the world, some different thin-slab casting processes have been developed. The first and foremost of these processes to be commercialized will be focused on here, the SMS Schloemann-Siemag AG process, which was commercialized at Nucor Steel. In this process, the liquid steel enters a vertical-type chromium-zirconium copper mold with a funnel-shaped bulge in the middle of the meniscus region. The bulge allows the introduction of the casting nozzle (Figure 1.1). The end of the funnel is rectangular, with an internal thickness of about 50 mm (1), corresponding to the slab thickness. With the exception of the funnel-shaped mold, the components of the machine are similar to standard continuous casting equipment (2).

The slab enters a gas-fired tunnel furnace after solidification and is allowed to equilibrate to the initial rolling temperature. Figure 1.2 shows a schematic of the overall process. After exiting the tunnel soaking furnace, the slab is processed in a multi-stand hot-strip mill, and coiled.

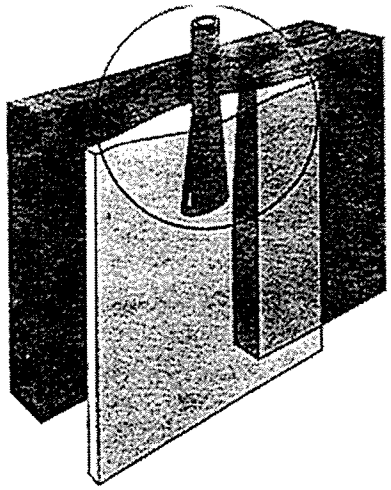

Figure 1.1 Funnel-shaped mold with submerged casting nozzle (3).

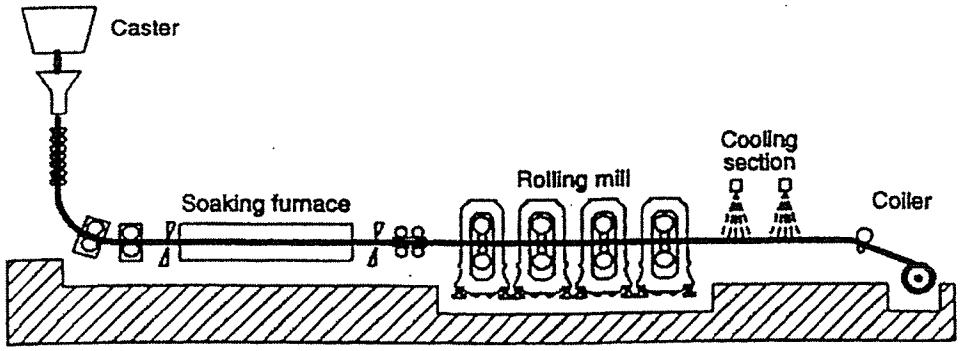

Figure 1.2 Schematic representation of thin-slab casting process (4).

1.2.2 Casting of Liquid Steel

In traditional continuous casting, a high degree of superheat above the liquidus is reported to be unfavorable; as it leads to a more columnar structure instead of the preferred equiaxed structure (2). Thin-slab casting has a higher rate of solidification compared to conventional

casting. A 50 mm thin-cast slab can solidify within 90 seconds, while a 200 mm conventional cast slab takes approximately 15 minutes. The relationship between secondary dendrite arm spacing, λ_2, and the local solidification time, t_f, has been used (4) to quantify the increased solidification rates with the following equation:

$$\lambda_2 = A(Mt_f)^{1/3} \qquad [1.1]$$

where M is a constant depending on alloy composition. Increasing the solidification rate creates a finer as-cast structure. Experimental data showed that the secondary dendrite arm spacing was reduced from 300 mm in a 230 mm slab to 95 mm in a 50 mm slab (5). One study (7) suggests that the rapid solidification rate suppresses the precipitation of aluminum nitrides, which will be discussed in greater detail. These increased cooling conditions also make it possible to obtain fine TiN precipitates, as small as 10 nm (6). These particles are thought to be effective in pinning austenite grain boundaries during recrystallization controlled rolling (4).

Liquid steel composition is critical in thin-slab casting because the rate of heat extraction from the mold is higher than that of conventional casting. This leads to higher surface tensile strains from the thermal gradients in the solidifying shell of the slab. These strains may lead to longitudinal facial cracking (4). Composition issues make scrap quality control important in electric arc furnace mini-mills, as there is difficulty in economically removing tramp elements from the scrap through current refining processes. Difficulties in continuously casting HSLA slabs within the peritectic range of 0.07% to 0.15% carbon have also led to the typical practice of limiting the carbon content to levels below about 0.06% C (3).

The high casting speeds and size of the casting mold present additional challenges. Transverse corner cracks appearing within 75 mm of the corner of the slabs have been reported. Wigman and Millet (8) suggest this problem is due to the precipitation of AlN in regions of the slab that have fallen below the Ar_3. Below the Ar_3 temperature, ferrite begins to form at the austenite grain boundaries, lowering the ductility of the slab over a range of temperatures, forming a "ductility trough." The precipitation of the AlN in the ferrite locally embrittles the microstructure, and extends the ductility trough to lower temperatures (3). Turkdogan is cited as

suggesting that this precipitation is promoted by strain associated with the two-dimensional heat flow, causing the slab to be colder at the corners than the mid-face zone (3).

Another potential problem is the aforementioned longitudinal facial cracking. This problem may be closely related to the sulfur content of the steel (8). The sulfur content is important because of its influence on ductility near the solidification temperature. Sulfur segregates between solidifying dendrites and depresses the freezing range of the steel. This creates a liquid film in the interdendritic region, which is susceptible to dendritic separation and hot tears at low tensile strains. These surface tensile strains during slab bending are proportional to the slab thickness; thus thinner slabs may be better able to tolerate a greater loss of ductility than conventionally cast slabs (4).

1.2.3 Solid-State Processing

After straightening, the slabs are typically direct charged (i.e. not cooled and reheated) into the tunnel furnace. This direct charging of the steel is important in several respects. The direct charging saves considerable energy, and therefore cost in that the steel does not have to be reheated to temperature, with an order of magnitude difference in energy needed for the process (4). The potential benefit in energy savings is offset by another important consideration in direct charging, the absence of a γ–α–γ transformation to refine the grain size. A roughing roll applied directly after solidification is reported to be helpful when followed by recrystallization, by refining the as-cast structure and contributing to grain refinement as in the Mannesman process (4).

The slabs in the SMS process are direct charged from the tunnel furnace into hot rolling stands without roughing. Figure 1.3 provides insight into the processing response of the austenite, showing recrystallization response as a function of starting grain size for three different rolling reductions (30, 40, and 50 %) with interpass times of 1 and 2 seconds. According to the figure, heavy rolling reductions of 50% or more per pass are necessary to achieve full recrystallization between stands with an interpass time of two seconds over the widest range of initial austenite grain sizes (4). Figure 1.4 shows the refinement of austenite grain size as a slab is hot-rolled; it has been found that due to the coarse as-cast microstructure, full recrystallization does not occur in

the first pass of the finishing mill. Nonetheless, the overall reduction is somewhat higher than conventional hot-strip mills, and therefore the final grain size may be finer in the end product (9).

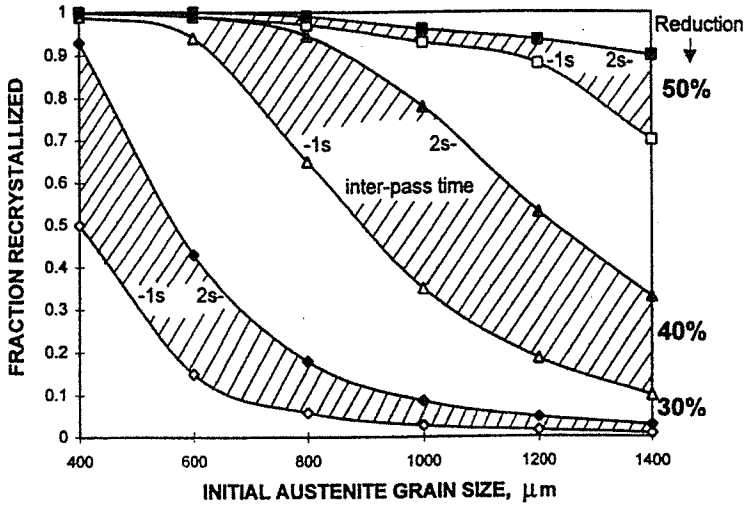

Figure 1.3 Effect of deformation on degree of recrystallization of coarse austenite for interpass times of one or two seconds (4).

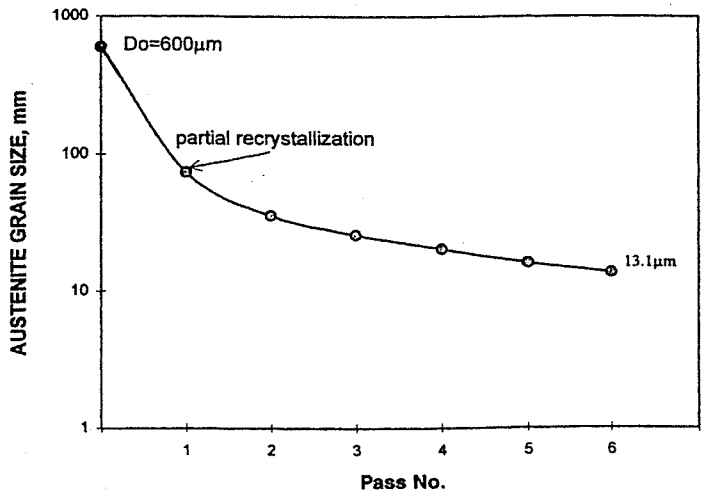

Figure 1.4 Austenite evolution during hot rolling of 50mm thick slab to a final thickness of 6 mm (adapted from 4).

1.3 Titanium Nitride Technology

Titanium has a low solubility in austenite, and therefore titanium nitride (TiN) exhibits a relatively slow particle coarsening rate (10). With low solubility, titanium nitrides tend to form at high temperatures making them a good candidate for examining precipitate formation near the solidification temperature, where differences between conventional slab casting and thin-slab casting should be most pronounced. At these temperatures, the effects of the increased post-solidification cooling rate associated with thin-slab casting can be studied. The low solubility prevents the use of TiN as an effective precipitation strengthening agent, but makes it particularly suitable for use as a grain refining precipitate at high temperatures. Small amounts of titanium can be added to steel in order to form a fine dispersion of TiN precipitates when continuously cast (6). These TiN particles have been shown to retard austenite grain boundary migration (4). The presence of particles on the grain boundary decreases the grain boundary area and therefore the boundary energy. By pinning the grain boundaries with increasingly stable precipitates, the austenite grain coarsening temperature is increased and the austenite grain size can be controlled during conventional slab reheating (see Figure 1.5, for example). Another study has shown austenite grain coarsening temperatures to be around 1200 °C (2192 °F) (11).

Zener proposed a relationship between the particle radius (r), the austenite grain radius (R), and the volume fraction of the pinning particles (f) (10):

$$R = \frac{4}{3} \cdot \frac{r}{f} \qquad [1.2]$$

This relationship means that a fine austenite grain size is maintained with either a large volume fraction of TiN particles or a smaller fraction of finer particles. This behavior is illustrated in Figure 1.6, where three independent models, the Zener model and two similar models, for the effects of particle size and volume fraction on grain size show the same general trend. The differences between predicted size are due to differences in assumptions of the models. It should be noted that obtaining both the maximum volume fraction and the finest dispersion of particles at the same time may not be practical during commercial processing. High Ti contents which would allow for large volume fractions are typically avoided because coarse TiN particles form in the liquid steel (10). These coarse particles are ineffective as grain refiners. A smaller volume fraction

of finer TiN precipitates is widely accepted as the best approach for austenite grain control. This will yield grain refinement and a stable austenite grain structure due to low grain boundary mobility (10).

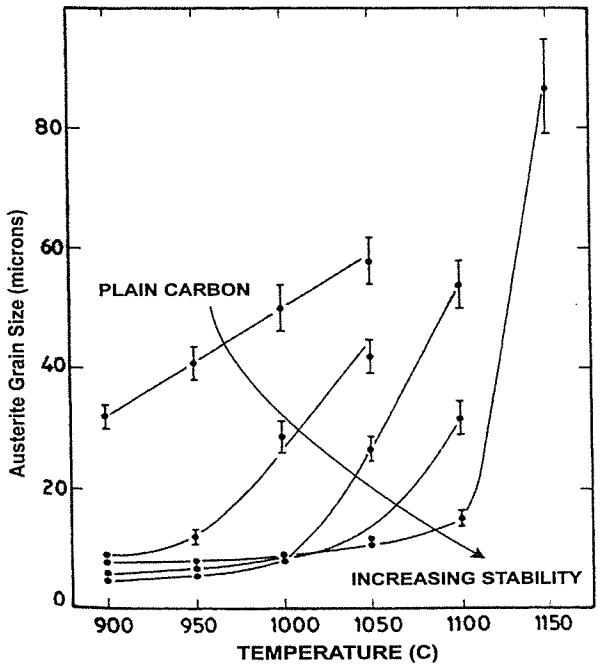

Figure 1.5 Increasing microalloy additions increase grain coarsening temperature (adapted from 12).

Using the Gladman equation, which will be described in more detail later, it is generally thought that the TiN particles must be less than about 50 nm in size in order to inhibit growth (14). These small precipitates are obtained by using low concentrations of Ti in the steel. The low concentrations prevent precipitation in the interdendritic liquid which would yield larger particles that are less effective for grain control. Particles formed by precipitation at lower temperatures in the solid state are the most effective for grain size pinning. If the particles form in the solid state, they are less likely to coarsen beyond the critical size for effectively pinning the austenite grain boundaries. Cooling rates also affect how the particles form, with faster solidification rates causing precipitation in the solid state. It has been shown that increasing the post-solidification

cooling rate refines the TiN particle size (Figure 1.7). Thus, TiN technology is better suited to continuously cast steels than ingot-cast steels (14). Thin-slab casting, with cooling rates greater than that of conventional casting, may have the potential for even finer TiN precipitates, and is thus the subject of this investigation.

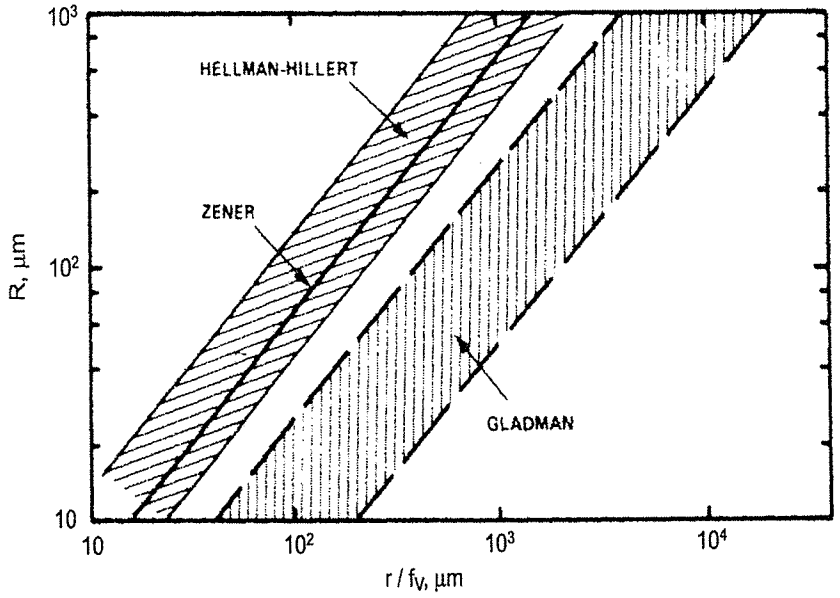

Figure 1.6 General relationship between grain size, R, particle size, r, and volume fraction, f_v, as predicted by three models (13).

The titanium and nitrogen concentrations in the steel should also be considered in the context of the carbon content. The carbon content, in large part, controls the solidification temperature, with higher carbon levels associated with lower liquidus and solidus temperatures. With increasing carbon content an increasing amount of (coarse) TiN is conceivably formed in the liquid, where TiN solubility is greater. Coarse TiN precipitates have been noted to be ineffective with regard to the control of austenite grain size. In lower carbon steels, less TiN may form in the liquid because of the higher liquidus temperature (10).

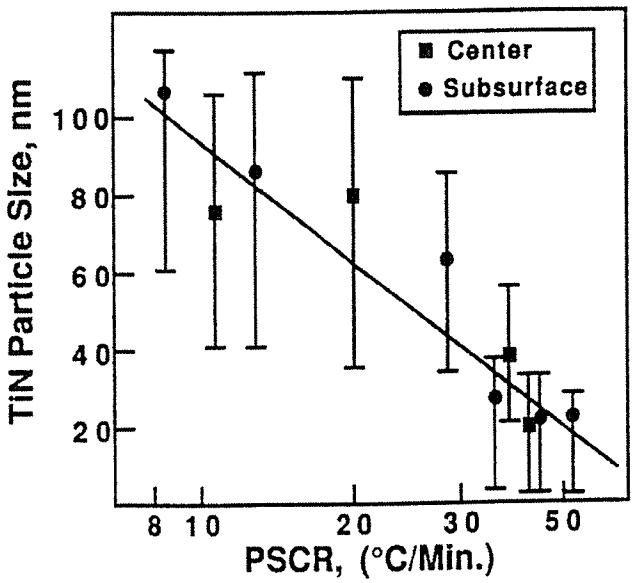

Figure 1.7 Effect of post-solidification cooling rate on TiN particle size (14).

Once formed, TiN coarsening can be minimized by lowering the concentration of titanium left in solution in the austenite (15). Increasing the nitrogen to achieve a hypostoichiometric Ti:N ratio is utilized for this purpose (10). Figure 1.8 shows a TiN solubility diagram. The figure shows that moving away from the stoichiometric line by increasing the nitrogen in the steel decreases the amount of titanium in the system after precipitation occurs during cooling. During precipitation, the solute Ti and N levels move down along a line parallel to the stoichiometric line. The two curves marked with temperatures are lines of constant solubility or driving force. The lines represent combinations of solute Ti and N that are in equilibrium with TiN at the indicated temperature.

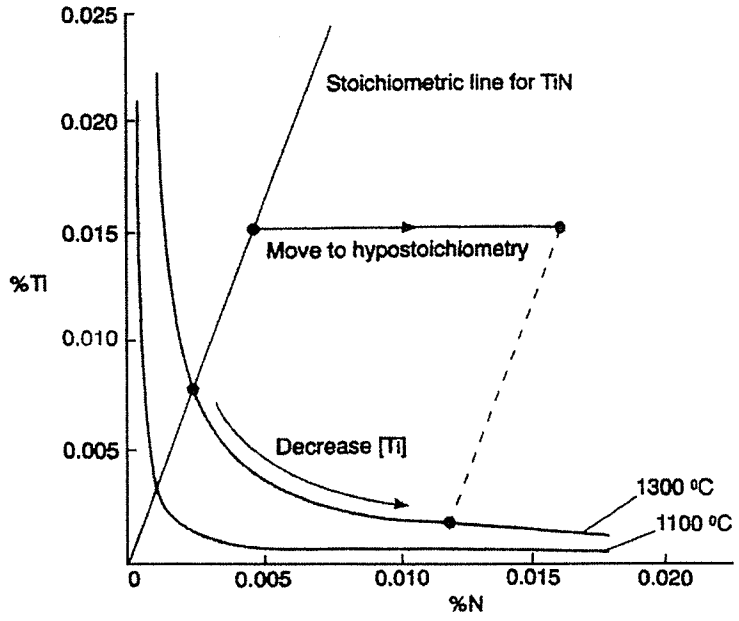

Figure 1.8 Solubility diagram showing how moving to a hypostoichiometric Ti:N ratio will decrease the amount of titanium left in solution (10).

The titanium nitride particles can grow by Ostwald Ripening during post solidification cooling and heat treatments. The Wagner equation describes the kinetics of particle coarsening, taking both time and temperature into account:

$$r_t^3 - r_o^3 = \frac{8\sigma D[M]V}{9GT} \cdot t \qquad [1.3]$$

where r_t is the particle radius at t, r_o is the particle radius at time t = 0, σ is the particle/matrix interfacial surface energy, D is the diffusivity of the rate controlling specie (Ti) in the austenite matrix, [M] is the concentration of Ti in the matrix, V is the particle molar volume, G is the universal gas constant, T is the temperature in Kelvin, and t is time (14). The Wagner equation shows the TiN particle coarsening rate will be reduced in proportion to the decrease in titanium left in solution. As mentioned above, moving to a hypostoichiometric Ti:N ratio should minimize TiN

particle coarsening during post-solidification processing (14). Pickering (10) noted that "the grain coarsening temperature, other factors being equal, will be highest for the greatest volume fraction of pinning particles," and that it might be expected that "the maximum grain coarsening temperature would occur at the stoichiometric ratio where the temperature dependence of solubility is greatest." Figure 1.9 shows that increasing only Ti or N from a stoichiometric composition may lead to the formation of particles at a higher temperature. The increased total volume fraction of particles is related to the length of the line between the Ti:N composition and the solubility line of interest (i.e. longer lines means more Ti and N have been used to form TiN precipitates). These concepts provide the basis for "conventional" TiN technology, and a primary objective of the present work is to assess whether or not the same priorities are applicable to thin-slab cast steels. For example, because faster cooling is associated with shorter times at high temperature, it was considered possible that particle coarsening considerations may be less important in thin-slab cast products.

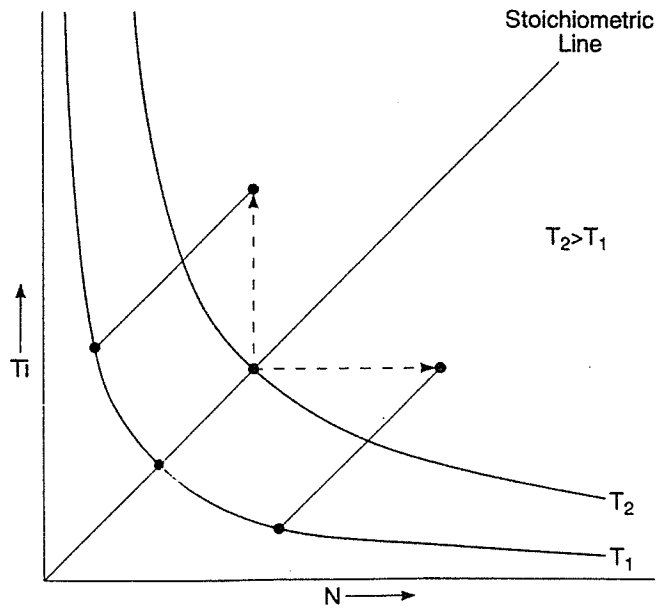

Figure 1.9 Solvus temperature of precipitates increase as composition moves away from stoichiometric line (10).